Mechanics of Advanced Composite Structures 10 (2023) 233 – 246

Semnan University

Mechanics of Advanced Composite Structures

journal homepage: http://MACS.journals.semnan.ac.ir

Modeling the Buckling Characteristics of Pineapple Leaf Fibre Reinforced Laminated Epoxy Composites

P. P. Borah, S. Kashyap *, S. Banerjee, S. Kirtania

Department of Mechanical Engineering, Tezpur University, Napaam, Sonitpur, 784028, Assam, India

KEYWORDS

Pineapple leaf fibre;
E-glass fibre;
Buckling analysis;
Finite element modeling.

ABSTRACT

Pineapple leaf is a natural fibre possessing superior mechanical strength which can be used as a reinforcing component in natural fibre-based composites. In general, composites can endure a wide variety of loads while in service. This work reports the buckling analysis of pineapple fibre reinforced epoxy composites and compared it to an isotropic composite reinforced with a synthetic fibre such as E-glass. The effects of changing the fibre volume fraction and plate aspect ratio, on physical buckling behaviour have been reported. The elastic parameters were calculated analytically, whereas the buckling studies were carried out using the finite element method. Buckling was shown to be significantly influenced by the changes in volume fractions, plate aspect ratio, and buckling mode. Additionally, the influence of design parameters such as optimum ply angle for composite stacking-sequence was also investigated under no shear conditions. It was observed that pineapple leaf fibre composites yielded better buckling characteristics than contemporary synthetic E-glass fibre composites.

1. Introduction

Natural fibre composites are being used to replace most structural applications in today's world, whether in the automation, aviation, or shipping industries. Because synthetic fibres are non-biodegradable and only reusable up to a certain point, their widespread use has had a negative and damaging influence on sentient beings. Natural fibres are crucial as they are biocompatible and biodegradable, have a high strength-to-weight ratio, have less density, and are non-toxic. Additionally, they are also abundantly available as most of the parts of fruits and plants are wasted due to a lack of knowledge regarding their economic value [1,2]. Natural fibres have recently been used in industrial and automation applications, although they still lack some of the properties that synthetic fibres can supply. Senthilkumar *et. al.* [1] analysed pineapple leaf fibre composite for free vibration and damping properties. Earlier, Saha et. al. investigated the mechanical, thermal, and biodegradation behaviour of pineapple leaf particulates and found satisfactory results [2]. Peças *et. al.* [3] reviewed several papers based on the usage of fibres in various industries and on their processing and utilisation in automotive industries. Mohammed *et. al.* [4] presented various surface treatment methods and the impact of chemical treatments on fibre matrix adhesion, along with the physical and mechanical characteristics of several fibres. Jawid *et. al.* [5] presented various properties and qualities of pineapple leaf fibres. They also stated that pineapple leaf fibres are extensively used in textile industries and automation industries. Sema *et. al.* [6] provided insight into pineapple leaf fibres cultivation and their availability in portions of northeast India such as Karbi Anglong, North Cachar hills, West and East Garo hills, and Barak valley which produces almost 40% of the total pineapple of India. Mishra *et. al.* [7] investigated the fibre loading condition and its impact resistance for pineapple leaf fibre composites for various weight fractions. It was found that these composites have an impact strength of around 80.29 J/m for a 30% weight fraction. Borah *et. al.* [8] studied the structural responses of various fibre composites and

* Corresponding author. Tel.: +91-7002705174
E-mail address: satadru@tezu.ernet.in

DOI: 10.22075/macs.2022.28005.1425
Received 2022-08-04; Received in revised form 2022-11-16; Accepted 2022-12-24.

presented a comparative study for varying damping ratios with plate aspect ratio and volume fractions. Jalili *et. al.* [9] investigated the effects of flax fibre on the multi-objective optimum design of hybrid laminated composite for maximum buckling with different material configurations keeping the cost as a priority. Hosseinzadeh *et. al.* [10] conducted the multi-objective optimization for flax fibres composite by minimizing the cost and maximizing the frequency gaps in order to assess the capabilities of fibre-reinforced composites. Le *et. al.* [11] investigated the viscoelastic beahviour of a laminated composite under axial loading conditions using Abaqus. Le *et. al.* [12] studied the buckling behaviour of transversely isotropic multilayered beams with thin and soft interfaces for a better understanding of wrinkle formation under compressive loading. Chai *et. al.* [13] presented the stability behaviour of typical laminated composite plates with all sides simply supported and bound to in-plane stress conditions, utilising a total potential energy method in conjunction with the Rayleigh-Ritz technique. Darvizeh *et. al.* [14] investigated the buckling of composite plates, wherein the mathematical modeling for typically laminated plates was constructed using the generalized differential quadrature rule (GDQR) and the R–R approach. Adali *et. al.* [15] stated that if the plies are symmetric about the middle, a balanced laminated is achieved where the coupling is absent. This implies that a balanced configuration has the advantage of reducing the D_{16} and D_{26} values for any angle ply laminates as these values can be neglected and are considered zero. Furthermore, they also mentioned that for laminates with several layers, D_{16} and D_{26} values might be rather modest in comparison to other D_{ij} values. Bert *et. al.* [16] found that among various stacking sequences, simply supported plates and symmetrical angle ply laminates had the largest buckling mode under uni-axial and bi-axial loads. There has been a lot of research done on the mechanical and thermal properties of natural fibres, however, relatively little attention has been devoted to the structural deformations that may occur as a result of loading in composites.

The overall aim of this research is to investigate the buckling modes of failure of pineapple leaf fibre composite as a function of varying stacking sequences. Additionally, the buckling characteristics of the pineapple leaf fibre composites are compared with a synthetic fibre composite in order to understand the performance capabilities of natural fibre composites under buckling. The numerical analysis is performed using Kirchhoff's plate theory and Navier's solutions under no-shear conditions. Furthermore, buckling characteristics were modelled by FEM analysis.

The rest of the paper is organized as follows: Section 2 formulates the numerical method and theory for buckling. Additionally, it describes the boundary conditions applied and the modeling of laminated composite incorporating the applied loads. In section 3, the detailed outcomes have been explained, and finally, concluding remarks regarding the outcome of the research have been stated in section 4.

2. Problem Description and Experimental Setup

The elastic modulus, shear modulus, and Poisson's ratio of a composite lamina were calculated using the rule of mixture, as given by Jones [17]. The requisite fibre qualities were derived from several studies.

$$E_{11} = E_f V_f + E_m V_m \tag{1}$$

$$E_{22} = \frac{E_f E_m}{E_m V_f + E_f V_m} \tag{2}$$

Major Poisson's ratio (ν_{12}) and Minor Poisson's ratio (ν_{21}) can be obtained as;

$$\nu_{12} = \nu_f V_f + \nu_m V_m \tag{3}$$

$$\nu_{21} = \nu_{12}(\frac{E_{22}}{E_{11}}) \tag{4}$$

In-plane shear modulus (G_{12}) of the composite can be obtained as;

$$G_{12} = \frac{G_m G_f}{G_m V_f + G_f V_m} \tag{5}$$

where G_f, G_m are the shear modulus of fibre and matrix respectively and can be calculated as;

$$G_f = \frac{E_f}{2(1+\nu_f)}; \quad G_m = \frac{E_m}{2(1+\nu_m)} \tag{6}$$

In recent years, the usage of composites in structural applications has expanded dramatically. These composites are in the form of thin laminates that may be formed according to the pattern that is required. When thin laminates with no out-of-plane loads are examined, the lamina is regarded to be in a plane stress state, *i.e.*, $\sigma_3 = 0$, $\tau_{31} = 0$and $\tau_{23} = 0$. This yields the S_{ij}values which are known as reduced compliance coefficients. The compliance matrix [$\boldsymbol{S}$], inverting the compliance matrix [$\boldsymbol{S}$]and the reduced stiffness matrix [$\boldsymbol{Q}$]is obtained as shown by Jones [17];

$$\begin{bmatrix} \boldsymbol{\sigma_1} \\ \boldsymbol{\sigma_2} \\ \boldsymbol{\tau_{12}} \end{bmatrix} = \begin{bmatrix} \boldsymbol{Q_{11}} & \boldsymbol{Q_{12}} & \boldsymbol{0} \\ \boldsymbol{Q_{12}} & \boldsymbol{Q_{22}} & \boldsymbol{0} \\ \boldsymbol{0} & \boldsymbol{0} & \boldsymbol{Q_{66}} \end{bmatrix} \begin{bmatrix} \boldsymbol{\epsilon_1} \\ \boldsymbol{\epsilon_2} \\ \boldsymbol{\gamma_{12}} \end{bmatrix} \tag{7}$$

$$Q_{11} = \frac{E_{11}}{1 - \nu_{12}\nu_{21}} \tag{8}$$

$$Q_{12} = \frac{\nu_{12}E_{22}}{1 - \nu_{12}\nu_{21}} \tag{9}$$

$$Q_{22} = \frac{E_{22}}{1 - \nu_{12}\nu_{21}} \tag{10}$$

$$Q_{66} = G_{12} \tag{11}$$

where, Q_{ij} are called reduced stiffness coefficients, and are related to elastic constants as explained in [17]. A*2D* coordinate system is used to represent an angle lamina as shown in Figure 1. The axes displaying coordinate systems *1-2* are referred to as local axes, whereas the axes *x-y* are referred to as global axes. The angle formed by two axes is denoted by the symbol θ. The local and global stresses are related through transformation matrix T as described by Jones [17];

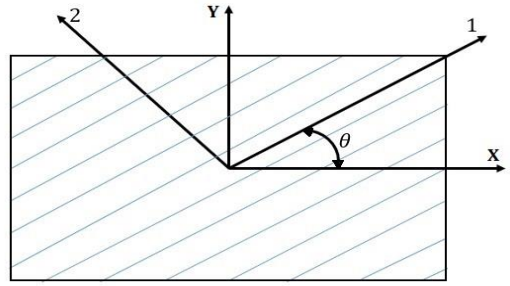

Fig. 1. Local and global axes of an angle lamina

The expression of global stress and global strain can be written as given by Jones [17];

$$\begin{bmatrix} \boldsymbol{\sigma_x} \\ \boldsymbol{\sigma_y} \\ \boldsymbol{\tau_{xy}} \end{bmatrix} = \begin{bmatrix} \overline{\boldsymbol{Q}}_{\boldsymbol{11}} & \overline{\boldsymbol{Q}}_{\boldsymbol{12}} & \overline{\boldsymbol{Q}}_{\boldsymbol{16}} \\ \overline{\boldsymbol{Q}}_{\boldsymbol{12}} & \overline{\boldsymbol{Q}}_{\boldsymbol{22}} & \overline{\boldsymbol{Q}}_{\boldsymbol{26}} \\ \overline{\boldsymbol{Q}}_{\boldsymbol{16}} & \overline{\boldsymbol{Q}}_{\boldsymbol{26}} & \overline{\boldsymbol{Q}}_{\boldsymbol{66}} \end{bmatrix} \begin{bmatrix} \boldsymbol{\epsilon_x} \\ \boldsymbol{\epsilon_y} \\ \boldsymbol{\gamma_{xy}} \end{bmatrix} \tag{12}$$

where, $\bar{Q}_{ij}$ elements are called transformed reduced stiffness matrix. The $\bar{Q}_{ij}$ elements can be found as given by Jones[17].

The location of laminas in the composite laminate is shown in figure 2.

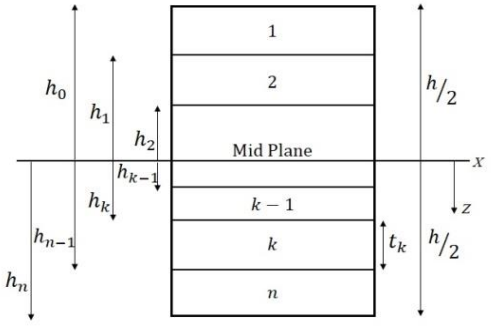

Fig. 2. Locations of laminas in a laminate

For the orientation of fibres in a stacking sequence of laminas in a different direction, the flexural stiffness $D_{ij}$and bending stiffness matrix [$\boldsymbol{D}$] are calculated as follows [18];

$$D_{ij} = \frac{1}{3}\sum_{k=1}^{n}[\overline{Q}_{ij}]_k(h_k^3 - h_{k-1}^3) \tag{13}$$

$$[\boldsymbol{D}] = \begin{bmatrix} \boldsymbol{D_{11}} & \boldsymbol{D_{12}} & \boldsymbol{D_{16}} \\ \boldsymbol{D_{12}} & \boldsymbol{D_{22}} & \boldsymbol{D_{26}} \\ \boldsymbol{D_{16}} & \boldsymbol{D_{26}} & \boldsymbol{D_{66}} \end{bmatrix} \tag{14}$$

2.1. Theory of Buckling

Equation of motion in terms of displacements in a constitutive relationship for a laminated plate in full matrix form can be written as shown by Chai and Hoon[13]:

$$\begin{bmatrix} \boldsymbol{N} \\ \boldsymbol{M} \end{bmatrix} = \begin{bmatrix} \boldsymbol{A} & \boldsymbol{B} \\ \boldsymbol{B} & \boldsymbol{D} \end{bmatrix} \begin{bmatrix} \boldsymbol{\varepsilon^0} \\ \boldsymbol{\varepsilon^1} \end{bmatrix} \tag{15}$$

where, $\varepsilon^0$and $\varepsilon^1$are called the membrane strains and surface curvatures respectively [13].

For a given plate, the total loss in potential energy of the deformed plate is taken from Chai and Hoon [13]:

$$\Pi = U - V \tag{16}$$

Using the strain energy displacement resultants and consecutive relations for the laminated plate by using the above expressions and solving the form given in Eq. 15 and substituting in Eq. 16 the strain energy as given by [13]:

$$\begin{aligned} U = & \\ & \frac{1}{2}\int_{\Omega}\{D_{11}\left(\frac{\partial^2 w_0}{\partial x^2}\right)^2 + 2D_{12}\left(\frac{\partial^2 w_0}{\partial x^2}\right)\left(\frac{\partial^2 w_0}{\partial y^2}\right) \\ & + 4D_{66}\left(\frac{\partial^2 w_0}{\partial x\,\partial y}\right)^2 + D_{22}\left(\frac{\partial^2 w_0}{\partial y^2}\right)^2 \\ & + 4D_{16}\left(\frac{\partial^2 w_0}{\partial x^2}\right)\left(\frac{\partial^2 w_0}{\partial x\,\partial y}\right) \\ & + 4D_{26}\left(\frac{\partial^2 w_0}{\partial y^2}\right)\left(\frac{\partial^2 w_0}{\partial x\,\partial y}\right)\}\,\mathrm{d}\Omega \end{aligned} \tag{17}$$

where, D_{ij} are reduced flexural stiffness values and $d\Omega = \mathrm{dxdy}$.

Assuming that the plate is subjected to stress resultants $\bar{N}_x, \bar{N}_y, \bar{N}_{xy}$ the potential energy acquired as a consequence of external loading is stated in [13]:

$$\begin{aligned} V = & \\ & \frac{1}{2}\int_{\Omega}\{\overline{N}_x\left(\frac{\partial w_0}{\partial x}\right)^2 + \overline{N}_y\left(\frac{\partial w_0}{\partial y}\right)^2 \\ & + 2\overline{N}_{xy}\left(\frac{\partial w_0}{\partial x}\right)\left(\frac{\partial w_0}{\partial y}\right)\}\,\mathrm{d}\Omega \end{aligned} \tag{18}$$

According to Hamilton's variational principle, real displacements among permissible routes accompanied by a dynamical method as stated by Darvijeh [14] is given by,

$$\delta \int_{t_o}^{t_1} \Pi \mathrm{d}t = 0 \tag{19}$$

$$\delta\Pi = \delta U - \delta V = 0 \tag{20}$$

where δ is the initial variation and t_0, t_1 are specified times, upon applying Hamilton's principle for a mid-plane symmetric plate, $B_{ij} = 0$ with coupling terms *i.e.* $D_{16} = D_{26} = 0$, and neglecting the shear effects of loading $\overline{N}_{xy} = 0$. Under these conditions, the equation governing deflection is given by Reddy[19].

$$\begin{aligned} &D_{11}\left(\frac{\partial^4 w_0}{\partial x^4}\right) + 2(D_{12} + 2D_{66})\left(\frac{\partial^4 w_0}{\partial x^2\,\partial y^2}\right) \\ &+D_{22}\left(\frac{\partial^4 w_0}{\partial y^4}\right) = \overline{N}_x\left(\frac{\partial^2 w_0}{\partial x^2}\right) + \overline{N}_y\left(\frac{\partial^2 w_0}{\partial y^2}\right) \end{aligned} \tag{21}$$

To determine a non-zero deflection the in-plane forces are [19];

$$\overline{N}_x = -N_0,\ \overline{N}_y = -kN_0,\ k = \frac{\overline{N}_x}{\overline{N}_y} \tag{22}$$

where k is also known as the plate buckling constant.

2.2. The Navier's Solution

Navier's solutions are particularly useful for orthotropic laminates. The Navier solution makes use of two sinusoidal functions that meets the boundary condition in exact form. The number of waves in the two directions is a function of the solution, the dimensions of the plate, and the properties of the material as expressed in [19].

$$w_0(x, y) = W_{mn} sin(\alpha x) sin(\beta y) \tag{23}$$

Substituting Eq. 23 into Eq. 21 we obtain (for any m and n)

$$N_0(m, n) = \frac{d_{mn}}{(\alpha^2 + k\beta^2)} \tag{24}$$

For uni-axial compressions of a rectangular laminate, $k = 0$ and for bi-axial $k = 1$. Where,

$$\begin{aligned} d_{mn} &= D_{11}\alpha^4 + 2(D_{12} + 2D_{66})\alpha^2\beta^2 \\ &+D_{22}\beta^4 \end{aligned} \tag{25}$$

$$\alpha = \frac{m\pi}{a}\ ,\ \beta = \frac{n\pi}{b} \tag{26}$$

$$\begin{aligned} N_0(m, n) = \frac{\pi^2}{m^2 b^2}[&D_{11}m^4\left(\frac{b}{a}\right)^2 \\ &+ 2(D_{12} + 2D_{66})m^2n^2 \\ &+ D_{22}n^4(\frac{a}{b})^2] \end{aligned} \tag{27}$$

The smallest value of N_0, for any m, occurs for $n = 1$, [19]. Hence critical buckling load is a function of $\overline{N} = N_0(m)$. For Navier's solution, the non-dimensionalized buckling load is found using this formula as expressed in Reddy [19].

$$\overline{N} = N_0 b^2/(\pi^2 D_{22}) \tag{28}$$

2.3. Finite Element Method

The FEM modeling of fibre composite was carried out in ANSYS composite prepost for the design and stacking sequence of laminated composite. SHELL181 type element was used in the present FE analysis as the SHELL181 is pertinent for the analysis of thin to substantially thick shell structures. The SHELL181 element contains four nodes, each with six degrees of freedom.

The boundary condition of the square plate for the eigenvalue buckling analysis was considered as simply supported (SSSS) on all 4 edges. The plate edges were transformed to the nodal named selection, making it easier to define the boundary conditions at the extreme boundary limits of edges. The nodal displacement along the *z*-axis was zero for all four edges of the plate, rotation along the *y*-axis was fixed for the top and bottom nodal edges, and rotation along the *x*-axis was fixed for the left and right nodal edges of the plate. Two additional nodal-named selections were created on the plate, one in middle (considering plate coordinates) where displacement along *x,y* was zero at the center and the other nodal-named selection at the side edge along the *x*-axis where displacement along *y* was set to zero. Figure 3 shows the stacking sequence of the composite.

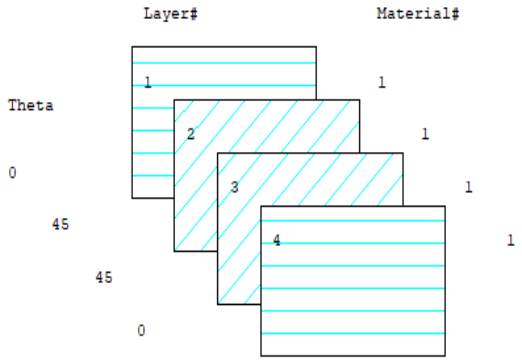

Fig. 3. Angle ply stacking sequence of $[0°/45°]s$

For the eigenvalue buckling analysis, the dimensions of the composite plate were kept at 120 mm × 120 mm × 1.6 mm based on ASTM standards as provided by Komur et. al. [20], where the ply thickness is 0.0004 meters or 0.4mm each, for 4 plies. For eigenvalue buckling in ANSYS, after applying the boundary condition, a load of 1000 N/mm (line pressure) was applied on the two opposite sides of the composite plate for uni-axial loading and on all four sides of the composite plate for bi-axial loading conditions of the simply supported plate (SSSS) (refer figures 4 and 5).

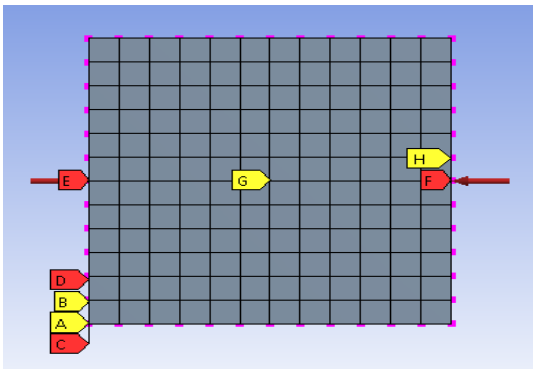

Fig. 4. Uni-axial loading of a square composite plate

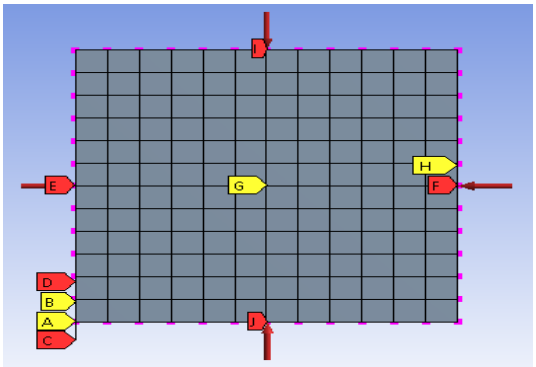

Fig. 5. Bi-axial loading of a square composite plate

The eigenvalue buckling in ANSYS gradually starts applying the load until it reaches the bifurcation point as shown in Figure 6 (A point where deformation occurs or starts).

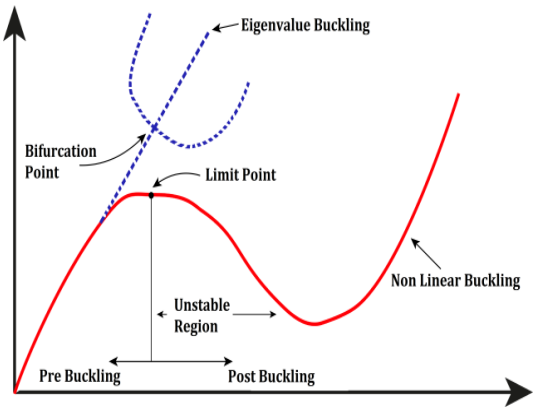

Fig. 6. Diagram for bifurcation point in buckling

At this point, the composite buckles, and the rest is examined in post-buckling behaviour, also known as nonlinear buckling. The loading of 1000 N/m is applied as a Load Multiplier or Load Factor, which is given as;

$$Ansys\ Load\ Factor\ Multiplier = \frac{Critical\ Buckling\ Load\ N_{cr}}{Applied\ Load}$$

The mesh convergence study was carried out and the optimal results were found for an element size of 12 mm mesh for 120 mm ×120 mm × 1.6 mm plate based on ASTM standards [20]. It had better mesh metric quality with an aspect ratio of 1 (best). There was no mesh refinement required as the plate considered was square or rectangular (for higher plate aspect ratios) and had no curvature to it, where the outcomes were identical with no or very minimal error. The plate wrapping factor details the wrap (mathematical deviation of a mesh element) of mesh elements. A greater wrapping factor means a lower or poorer quality mesh structure, and the ideal wrapping factor is 0. The mesh wrapping factor was 0 for the generated mesh in this study. By default, the element order was set to program controlled and physics preference was set to mechanical, thus for which ANSYS creates *quad 4* elements, and the number of elements and nodes were found to be 100 and 121 respectively.

3. Results and Discussion

It is one of the most critical aspects of failure analysis for a material that is undergoing deformation. Buckling is often determined in the situation of lengthy columns; although it can occur in the majority of practical instances, including thin flat plates. Buckling is a failure mode in which a structure deflects or deforms as a result of abrupt compressive force. This study uses Navier's model to investigate the impact of uni-axial and bi-axial loading under a given load on all four sides of an orthotropic composite plate. Navier's model is used for orthotropic plates with mid-plane symmetry and the effects of shear have been neglected. The variation of buckling load is studied with plate aspect ratio and the number of half waves in the *x*-direction. For the validation of the analytical result, the same values are considered as given in Reddy [19].

In Table 1, the influence of plate aspect ratio and modulus on non-dimensionalized buckling loads $\bar{N}$ of rectangular laminates $[0°/90°]s$ for uni-axial loading conditions ($k=0$) and bi-axial loading conditions ($k=1$) are shown, where, $\frac{E_{11}}{E_{22}} =$ varied, $G_{12} = G_{13} = 0.5E_{22}$, $G_{23} = 0.5E_{22}$, $\vartheta_{12} = 0.25$. All layers are considered to be of equal thickness [13].

Table 1. Comparison of Navier's non-dimensional buckling load [19] with the analytical result

		$\frac{E_{11}}{E_{22}}=5$		10		20		25		40	
k	$\frac{a}{b}$	Non dimensional	Numerical	Non dimensional	Numerical	Non dimensional	Numerical	Non dimensional	Numerical	Non dimensional	Numerical
0	0.5	13.9	13.85	18.12	18.09	21.87	21.85	22.87	22.85	24.59	24.57
	1	5.65	5.608	6.347	6.317	6.961	6.942	7.124	7.108	7.404	7.393
	1.5	5.233	5.191	5.277	5.247	5.31	5.291	5.318	5.32	5.332	5.321
1	0.5	11.12	11.08	12.69	12.63	13.92	13.88	14.24	14.21	14.76	14.73
	1	2.852	2.804	3.174	3.158	3.481	3.471	3.562	3.554	3.702	3.696
	1.5	1.61	1.597	1.624	1.614	1.634	1.628	1.636	1.631	1.641	1.637

In all cases the critical buckling mode is (m× n) = (1× 1), except for $\frac{a}{b}=0.5$and (k=1); for which the modes are (1× 1), (1× 2), (1× 2), (1× 2), and (1× 3) for modulus ratios 5, 10, 20, 25, and 40, respectively [19]. It was observed that larger aspect ratios resulted in increased modes of buckling, as seen in Figure 7.

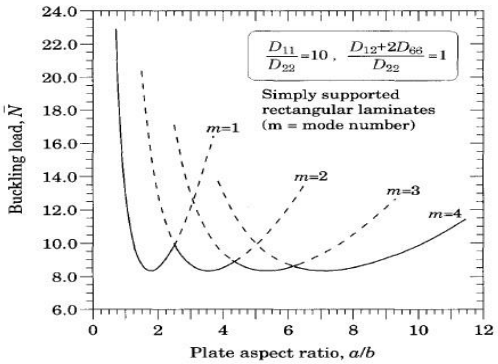

Fig. 7. Buckling load (non-dimensionalized), vs plate aspect ratio $\frac{a}{b}$ [19]

The non-dimensionalized buckling load $\bar{N}=N_0b^2/(\pi^2D_{22})$ versus plate aspect ratio $\frac{a}{b}$ for laminates with material parameters are $\frac{D_{11}}{D_{22}}=10$, $D_{12}+2D_{66}=D_{22}$are plotted in Figure 8.

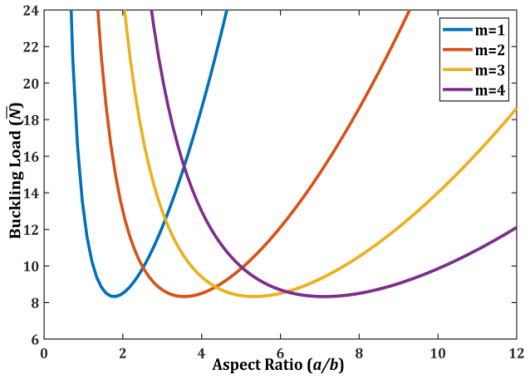

Fig. 8. Buckling load (non-dimensionalized), vs plate aspect ratio $\frac{a}{b}$ (numerical)

When the plate aspect ratio is less than 2.5, it collapses into a single half-wave in the x-direction (refer to Figure 9) [19].

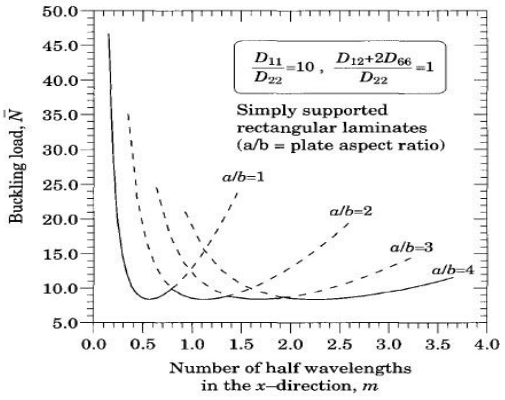

Fig. 9. Buckling load (non-dimensionalized) vs number of half wavelengths 'm' [19]

The plate bends into larger and more half-waves in the x-direction as the aspect ratio increases [19]. Notice that intersections of two successive modes correspond to specific aspect ratios (refer to Figure 10). As a result, there are two buckled mode configurations for each of these plate aspect ratios.

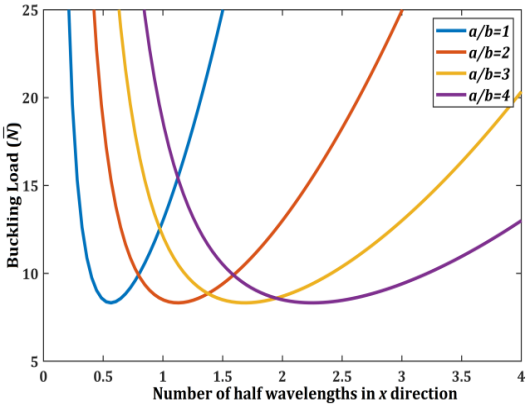

Fig. 10. Buckling load (non-dimensionalized) vs number of half wavelengths m [19] (numerical)

3.1. Comparison Between a Natural Fibre Composite and a Synthetic Fibre Composite Under Uni-axial Loading and Bi-axial Loading

Herein, PaLF composites are compared with a synthetic fibre composite (E-glass), as PaLF fibres have better mechanical properties compared to most of the other NF's [5]. For synthetic fibre, E-glass was considered as it had almost comparable mechanical properties with PaLF [5,21]. The fibre and matrix properties are shown in Table 2.

Table 2. Materials Properties

Fibres	Density ($\frac{kg}{m^3}$)	Young's Modulus (GPa)	Poisson's Ratio	References
Pineapple	1500	82	0.3	[3-5]
E-Glass	2500	73	0.22	[21]
Epoxy	1200	3.78	0.35	[8, 22]

Table 3 shows non-dimensionalized buckling load for uniaxial loading.

Table 3. $\bar{N}$ values for uni-directional loading

Stacking sequence	$\frac{a}{b}$	V_f %	PaLF		Min. buckling mode PaLF	E-Glass		Min. buckling mode E-glass	% change
			Numerical	FEM		Numerical	FEM		
[0°/0°]s	1	20	8.29	8.18	1 × 1	7.81	7.71	1 × 1	5.79
		25	9.43	9.31	1 × 1	8.83	8.71	1 × 1	6.36
		30	10.61	10.47	1 × 1	9.88	9.75	1 × 1	6.88
	2	20	8.18	8.05	1 × 1	7.81	7.71	1 × 1	4.52
		25	8.82	8.68	1 × 1	8.62	8.49	1 × 1	2.27
		30	9.53	9.38	1 × 1	9.28	9.13	1 × 1	2.62
	3	20	7.08	6.99	2 × 1	6.84	6.76	2 × 1	3.39
		25	7.78	7.69	2 × 1	7.48	7.39	2 × 1	3.86
		30	8.53	8.43	2 × 1	8.17	8.07	2 × 1	4.22
[0°/90°]s	1	20	8.28	8.09	1 × 1	7.81	7.62	1 × 1	5.68
		25	9.42	9.21	1 × 1	8.82	8.62	1 × 1	6.37
		30	10.60	10.36	1 × 1	9.87	9.65	1 × 1	6.89
	2	20	8.28	8.09	2 × 1	7.81	7.62	2 × 1	5.68
		25	9.42	9.21	2 × 1	8.82	8.62	2 × 1	6.37
		30	10.60	10.36	2 × 1	9.87	9.65	2 × 1	6.89
	3	20	7.90	7.70	2 × 1	7.56	7.37	2 × 1	4.30
		25	8.80	8.58	2 × 1	8.38	8.17	2 × 1	4.77
		30	9.74	9.51	2 × 1	9.23	9.01	2 × 1	5.24
[0°/45°]s	1	20	8.68	8.59	1 × 1	8.16	8.06	1 × 1	5.99
		25	9.91	9.82	1 × 1	9.26	9.16	1 × 1	6.56
		30	11.17	11.08	1 × 1	10.38	10.29	1 × 1	7.07
	2	20	8.66	8.59	2 × 1	8.14	8.06	2 × 1	6.00
		25	9.88	9.82	2 × 1	9.23	9.16	2 × 1	6.58
		30	10.96	10.86	1 × 1	10.36	10.29	2 × 1	5.47
	3	20	7.78	7.72	2 × 1	7.47	7.40	2 × 1	3.98
		25	8.65	8.60	2 × 1	8.25	8.19	2 × 1	4.62
		30	9.56	9.52	2 × 1	9.08	9.03	2 × 1	5.02
[0°/60°]s	1	20	8.57	8.45	1 × 1	8.06	7.94	1 × 1	5.95
		25	9.78	9.65	1 × 1	9.14	9.01	1 × 1	6.54
		30	11.02	10.89	1 × 1	10.25	10.11	1 × 1	6.99
	2	20	8.55	8.45	2 × 1	8.04	7.94	2 × 1	5.96
		25	9.75	9.65	2 × 1	9.11	9.01	2 × 1	6.56
		30	10.98	10.89	2 × 1	10.21	10.11	2 × 1	7.01
	3	20	7.89	7.80	2 × 1	7.56	7.47	2 × 1	4.18
		25	8.78	8.71	2 × 1	8.37	8.28	2 × 1	4.67
		30	9.71	9.65	2 × 1	9.21	9.14	2 × 1	5.15

From Table 3, the buckling load values for uni-axial loading for PaLF composite and E-glass composites can be obtained. The minimum buckling load for various stacking-sequence of $[0°/0°]s$, $[0°/90°]s$, $[0°/45°]s$ and $[0°/60°]s$ has been provided for increasing volume fraction. Variations for increasing plate aspect ratios and buckling load are also shown. According to Table 3, the buckling load values for higher plate aspect ratios occur at higher mode shapes. This is because, as previously stated in Eq. 27, the minimum critical buckling load is a function of 'm', and thus the minimum value for critical buckling may occur at higher mode shapes as the aspect ratio increases for certain values of modes.

It is certain that the PaLF composite outperforms the E-glass composite in terms of outcomes. For plate aspect ratio $(\frac{a}{b} = 1)$ and $(\frac{a}{b} = 1)$ at [0°/45°]s stacking sequence, the PaLF composite showed the best possible results. Similar findings were obtained for $\theta = 45°$ stacking sequence under uni-axial compression by [15,23].

Figure 11 shows the variation of non-dimensionalized buckling load to plate aspect ratio for increasing mode shapes. The figure also shows the variation for different stacking-sequence of the composite plate. It can be noted that the non-dimensionalized buckling load is minimum for [0°/90°]s stacking sequence, whereas the [0°/45°]s and [0°/0°]s stacking sequence results are better. Note that Figure 11 shows the non-dimensionalized form for a continuously varying plate aspect ratio.

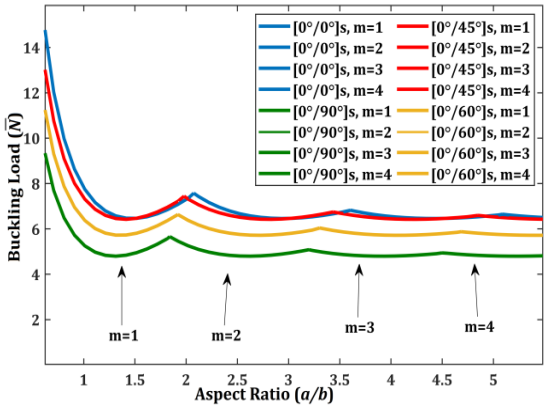

Fig. 11. Buckling load (Non-dimensionalised) vs plate aspect ratio for uni-axial loading of various stacking-sequence at 25% volume fraction of PaLF composite

Non-dimensionalized form $(\bar{N})$ is important in understanding the concepts of how this parameter $(\bar{N})$ is directly related to flexural stiffness values, for changing plate aspect ratios. It could not be possible to understand directly just by checking the critical buckling load values. As critical buckling values will show the possible load at which it will start to buckle and not the modes of buckling. The non-dimensionalized form could be used to study how a plate will behave under certain loads and in several modes that it will buckle into. The non-dimensionalized buckling load has an inverse relation to D_{22} as previously stated in Eq. 28. Also as stated by Joshi *et. al.* [23], at 90°, D_{11} equals the value of D_{22} at 0° and D_{22} at 90° equals the value of D_{11} at 0°. At 45°, D_{11} and D_{22} are equal, hence the maximum buckling load occurs at 45° orientation. But the inverse relationship between D_{22} and non-dimensionalized buckling load results in changing the maximum buckling load values for [0°/0°]sand [0°/90°]s stacking sequence. Furthermore, it can also be observed how increasing the plate aspect ratio changes the buckling mode for any plate. As the plate aspect ratio grows, the plate buckles into more and more half waves in the x-direction. It is worth noting that the intersection of two successive modes for various stacking sequences, happens at a particular mode and plate aspect ratio. For higher angles of orientation of fibres apart from [0°/0°]s stacking sequence, figure 11, shows how the plate buckles into two half waves as the plate aspect ratio reaches two.

Table 4 shows the buckling load values for bi-axial loading for the PaLF composite and E-glass composite.

For the bi-axial loading of the composite plate, it was observed that the minimum critical buckling load was lowered by a significant amount as compared to uni-axial loading. PaLF results are still better for comparison with E-glass fibre. The minimum critical buckling load for all stacking-sequence at different volume fractions and plate aspect ratios were found at $m = 1, n = 1$. Buckling load for bi-axial loading is unsustainable for a higher plate aspect ratio because the plate lengthens and the buckling load decreases drastically.

It was observed that PaLF composite would be much more resistant to deformation when compared to E-glass due to its superior mechanical properties. Thus PaLF can be a suitable alternative for E glass in different types of composites. When compared with synthetic fibre composites; PaLF composites showed better buckling characteristics, thus, showing that PaLF composites outperform contemporary E-glass composites. The improvements were observed to be more in the case of square laminates and at higher weight fraction of fibres (i.e. 30 vol%). Square PaLF composite plates with 30 vol% fibres showed a buckling load increment of approximately about 7% when compared with similar E-glass composites. Thus, PaLF composite materials have huge potential to be used in structural components under buckling conditions.

Table 4. $\bar{N}$ values for bi-directional loading

Stacking sequence	$\frac{a}{b}$	V_f %	PaLF		Min. buckling mode PaLF	E-Glass		Min. buckling mode E-glass	% change
			Numerical	FEM		Numerical	FEM		
[0°/0°]	1	20	4.15	4.09	1 × 1	3.91	3.85	1 × 1	5.78
		25	4.72	4.65	1 × 1	4.42	4.36	1 × 1	6.36
		30	5.30	5.23	1 × 1	4.94	4.87	1 × 1	6.79
	2	20	1.63	1.61	1 × 1	1.60	1.58	1 × 1	1.84
		25	1.75	1.74	1 × 1	1.72	1.70	1 × 1	1.71
		30	1.90	1.88	1 × 1	1.85	1.83	1 × 1	2.63
	3	20	1.32	1.30	1 × 1	1.31	1.29	1 × 1	0.76
		25	1.40	1.39	1 × 1	1.39	1.37	1 × 1	0.71
		30	1.50	1.48	1 × 1	1.48	1.46	1 × 1	1.33
[0°/90°]	1	20	4.14	4.04	1 × 1	3.90	3.81	1 × 1	5.80
		25	4.71	4.60	1 × 1	4.41	4.31	1 × 1	6.37
		30	5.30	5.18	1 × 1	4.93	4.82	1 × 1	6.98
	2	20	1.97	1.92	1 × 1	1.89	1.85	1 × 1	4.06
		25	2.18	2.13	1 × 1	2.08	2.04	1 × 1	4.59
		30	2.40	2.35	1 × 1	2.29	2.24	1 × 1	4.58
	3	20	1.72	1.69	1 × 1	1.66	1.63	1 × 1	3.49
		25	1.90	1.87	1 × 1	1.83	1.79	1 × 1	3.68
		30	2.09	2.05	1 × 1	2.00	1.96	1 × 1	4.31
[0°/45°]	1	20	4.34	4.29	1 × 1	4.08	4.03	1 × 1	5.99
		25	4.95	4.91	1 × 1	4.63	4.58	1 × 1	6.46
		30	5.59	5.54	1 × 1	5.19	5.14	1 × 1	7.16
	2	20	1.82	1.81	1 × 1	1.77	1.75	1 × 1	2.75
		25	2.00	1.98	1 × 1	1.93	1.91	1 × 1	3.50
		30	2.18	2.17	1 × 1	2.10	2.09	1 × 1	3.67
	3	20	1.48	1.46	1 × 1	1.45	1.43	1 × 1	2.03
		25	1.60	1.59	1 × 1	1.56	1.55	1 × 1	2.50
		30	1.73	1.72	1 × 1	1.69	1.67	1 × 1	2.31
[0°/60°]	1	20	4.29	4.22	1 × 1	4.03	3.97	1 × 1	6.06
		25	4.89	4.83	1 × 1	4.57	4.51	1 × 1	6.54
		30	5.51	5.44	1 × 1	5.12	5.06	1 × 1	7.08
	2	20	1.90	1.88	1 × 1	1.83	1.81	1 × 1	3.68
		25	2.09	2.07	1 × 1	2.01	1.99	1 × 1	3.83
		30	2.29	2.28	1 × 1	2.19	2.18	1 × 1	4.37
	3	20	1.59	1.57	1 × 1	1.54	1.52	1 × 1	3.14
		25	1.73	1.72	1 × 1	1.68	1.66	1 × 1	2.89
		30	1.89	1.88	1 × 1	1.83	1.81	1 × 1	3.17

Figure 12 shows the variation of non-dimensionalized buckling load to plate aspect ratio for increasing mode values m for bi-axial loading. It can be noted that buckling load decreases drastically for increasing plate aspect ratio($\frac{a}{b}$). This can also be viewed as, considering bi-axial loading the plate is exerted to compressive forces from all sides, thus making the plate easy to buckle, so at higher plate aspect ratios the buckling effect will be significantly more resulting in a lower value of buckling load.

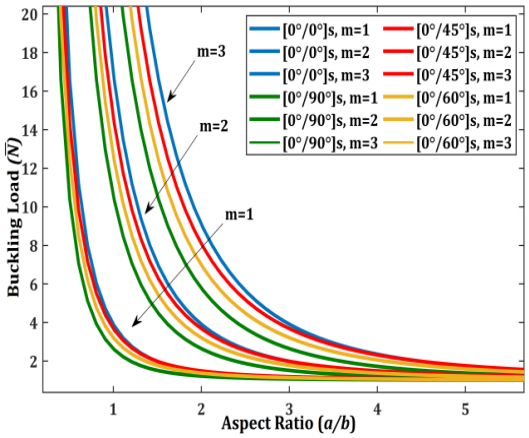

Fig. 12. Buckling load (Non-dimensionalized) vs plate aspect ratio for bi-axial loading of various stacking-sequence at 25% volume fraction of PaLF composite

It can be noted from figure 12 that, for higher values of plate aspect ratio the mode of buckling never shifts to higher modes, as the minimum buckling load for bi-axial loading occurs at $m = 1, n = 1$. Eq. 27 shows that non-dimensionalized buckling is strongly associated to b^2, and hence the dependency results in the minimal buckling mode.

Table 5 shows the variation of critical buckling load for uni-axial loading of a discrete array of stacking-sequence with changing plate aspect ratio at 25 vol% vol fraction for PaLF composite.

According to Joshi *et. al.* [23] for a square plate under uni-axial compression (Eq. 24) adds significantly to the buckling load. The bending stiffness coefficient D_{11}continues to fall as the orientation increases from 0° to 90°. As mentioned before, at 90°, D_{11}equals D_{22}at 0° and D_{22} at 90° equals D_{11} at 0°. At 45°, D_{11} and D_{22} are equal, hence the maximum buckling load occurs at 45° orientation. Also, Joshi *et. al.* [23] observed that if the plate aspect ratio $\frac{a}{b}$ is less than one, then the contribution of D_{22} decreases with decreasing aspect ratio and D_{11}strives to push the optimal fiber orientation toward 0°, while $D_{12} + 2D_{66}$ and D_{22} attempts to hold it back. As a result, the optimal fiber orientation is between 0°and45°. For an aspect ratio higher than one, D_{22} contributes significantly and attempts to pull the fibre orientation towards 90°, resulting in an effective fibre orientation between 45° and 90°. According to Joshi *et. al.* [23] changing the buckling mode to $m = 2, n = 1$, affects the contribution of each attribute in Eq. 27. Because D_{11} is multiplied by m^4, the D_{22} term no longer dominates at near-to-unity aspect ratios. This results in optimal fiber orientation angles ranging from 45°and 90° for aspect ratios in the range from one to two. As a consequence, nearly identical findings were achieved for this investigation, where the optimal fibre stacking sequence for increased plate aspect ratio was discovered to be for the [0°/60°]$s$stacking sequence.

Table 5. Variation of critical buckling load for uni-axial loading of a discrete array of stacking-sequence with changing plate aspect ratio at 25 vol% vol fraction for PaLF composite

$\frac{a}{b}$	[0°/0°]	Min. buckling mode $m \times n$	[0°/90°]	Min. buckling mode $m \times n$	[0°/45°]	Min. buckling mode $m \times n$	[0°/60°]	Min. buckling mode $m \times n$
0.2	142.440	1 × 1	128.597	1 × 1	133.008	1 × 1	130.175	1 × 1
0.4	37.682	1 × 1	34.228	1 × 1	35.926	1 × 1	35.070	1 × 1
0.6	18.494	1 × 1	17.062	1 × 1	18.184	1 × 1	17.725	1 × 1
0.8	12.028	1 × 1	11.420	1 × 1	12.255	1 × 1	11.970	1 × 1
1	9.309	1 × 1	9.209	1 × 1	9.817	1 × 1	9.652	1 × 1
2	8.684	1 × 1	9.209	2 × 1	9.817	2 × 1	9.652	2 × 1
3	7.689	2 × 1	8.583	2 × 1	8.601	2 × 1	8.708	2 × 1
4	7.787	3 × 1	8.356	3 × 1	8.584	3 × 1	8.598	3 × 1
5	7.845	3 × 1	8.372	4 × 1	8.699	4 × 1	8.668	4 × 1
6	7.689	4 × 1	8.434	5 × 1	8.601	4 × 1	8.708	4 × 1
7	7.712	5 × 1	8.409	5 × 1	8.556	5 × 1	8.606	5 × 1
8	7.757	5 × 1	8.356	6 × 1	8.584	6 × 1	8.598	6 × 1
9	7.689	6 × 1	8.353	7 × 1	8.601	6 × 1	8.626	7 × 1
10	7.695	7 × 1	8.372	8 × 1	8.558	7 × 1	8.625	7 × 1

Figure 13 shows the fluctuation of buckling load for uni-axial loading to increasing plate aspect ratio for various ply stacking sequences. When previously noted, the best ply angle for a plate aspect ratio of $\frac{a}{b} = 1$ & $\frac{a}{b} = 2$ was determined to be approximately 45° and as the plate aspect ratio increases the optimum ply angle shifted towards 90°.

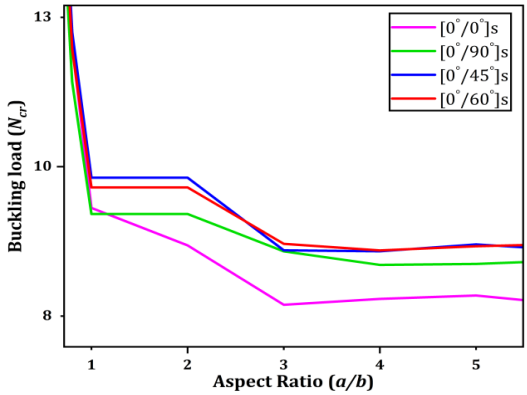

Fig. 13. Uni-axial buckling load vs plate aspect ratio for various stacking-sequence of PaLF composite at 25% volume fraction from Table 5.

This can be validated from figure 13 which shows that for larger plate aspect ratios, the optimal ply angle for uni-axial loads was about 60° for the aforementioned simulation results using 4 plies stacking-sequence. Joshi *et. al.* [23] found the best ply orientation angle for uni-axial loading at 50° while considering 6 plies stacking-sequence.

Now considering bi-axial loading in the composite plate for various stacking-sequence from Table 6, in conjunction with Figure 14, it can be seen that for bi-axial loading the [0°/45°]s stacking sequence performed best with a plate aspect ratio of one. When the plate aspect ratio exceeds one, the cross-ply stacking sequence of [0°/90°]s shows the best possible results compared to other stacking sequences. This is also true that the cross-ply stacking sequence is mostly considered for bi-axial loading in composite plates, as it can withstand a higher amount of loading. Hence it would be wise to go for [0°/90°]s stacking sequence under bi-axial loading in composites.

The uniaxial and biaxial loading of composites for critical buckling load study has been carried out considering the parameters that account for buckling as in Eq. 27. Figures 13 and 14 provide the information regarding the failure of a composite at the minimum value of buckling irrespective of mode, and depicts the change in plate aspect ratio to corresponding critical buckling.

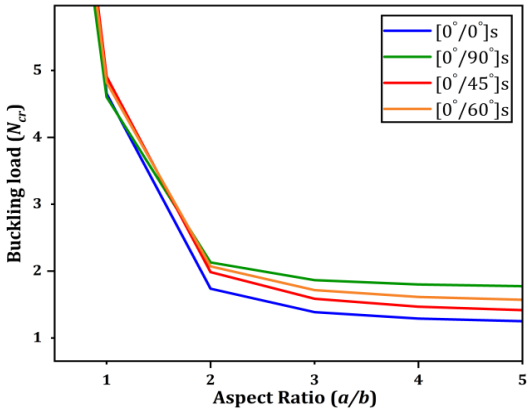

Fig. 14. Bi-axial buckling load vs plate aspect ratio for stacking-sequenceofPaLF composite at 25% vol. fraction

Table 6. Variation of critical buckling load for bi-axial loading of a discrete array of stacking-sequence with changing plate aspect ratio at 25% volume fraction for PaLF composite

$\frac{a}{b}$	[0°/0°]	Min. buckling mode $m \times n$	[0°/90°]	Min. buckling mode $m \times n$	[0°/45°]	Min. buckling mode $m \times n$	[0°/60°]	Min. buckling mode $m \times n$
0.2	136.9611	1 × 1	123.6507	1 × 1	127.8927	1 × 1	125.1684	1 × 1
0.4	32.4844	1 × 1	29.5073	1 × 1	30.9704	1 × 1	30.2325	1 × 1
0.6	13.5984	1 × 1	12.5458	1 × 1	13.3708	1 × 1	13.0329	1 × 1
0.8	7.3341	1 × 1	6.9632	1 × 1	7.4723	1 × 1	7.2986	1 × 1
1	4.6547	1 × 1	4.6045	1 × 1	4.9084	1 × 1	4.8262	1 × 1
2	1.7367	1 × 1	2.1296	1 × 1	1.9848	1 × 1	2.0701	1 × 1
3	1.3857	1 × 1	1.8651	1 × 1	1.5865	1 × 1	1.716	1 × 1
4	1.2892	1 × 1	1.7994	1 × 1	1.467	1 × 1	1.6139	1 × 1
5	1.25	1 × 1	1.7747	1 × 1	1.4158	1 × 1	1.5711	1 × 1
6	1.2303	1 × 1	1.7629	1 × 1	1.3893	1 × 1	1.5493	1 × 1
7	1.2191	1 × 1	1.7564	1 × 1	1.3737	1 × 1	1.5365	1 × 1
8	1.212	1 × 1	1.7524	1 × 1	1.3637	1 × 1	1.5284	1 × 1
9	1.2072	1 × 1	1.7498	1 × 1	1.357	1 × 1	1.523	1 × 1
10	1.2038	1 × 1	1.7479	1 × 1	1.3522	1 × 1	1.5192	1 × 1

This work describes the possibility of using a PaLF composite in assisting researchers in identifying practical prospective applications in the field of acoustic and vibration isolation such as multi-dimensional earthquake isolation devices using viscoelastic dampers and vibration isolation pads used in industries [4], impact energy absorption widely incorporated in motorsports and automotive application [4] and anti-crushing devices used in automotive applications, and super-light composite panels used in windmills and aerospace applications [4, 8]. The work could be further expanded to experimental findings. Additionally, this study can be broadly performed for different structures like honeycomb and stiffened structures considering the hybridization of composites.

4. Conclusions

The goal of the current study is to create an NF composite with enhanced buckling properties that can support axial loads without easily bending or deforming. Finite element analysis was used to perform buckling of thin laminated plates for the PaLF composite and compared it to an isotropic synthetic fibre like E-glass. Additionally, the model's correctness was determined by numerically comparing the findings. The generalized conclusions that can be drawn are as follows;

- It was observed that PaLF composite would be much more resistant to deformation when compared to E-glass due to its superior mechanical properties. Thus PaLF can be a suitable alternative for E-glass in different composites.
- In case of bi-axial loading of the composite plates, it was observed that the critical buckling load was lowered by a significant amount when compared to uni-axial loading conditions.
- When compared with synthetic fibre composites; PaLF composites showed better buckling characteristics, thus, showing that PaLF composites outperform contemporary E-glass composites. The improvements were observed to be more in the case of square laminates and at higher weight fraction of fibres (i.e. 30 vol%). Square PaLF composite plates with 30vol% fibres showed a buckling load increment of approximately about 7% when compared with similar E-glass composites.
- Considering uni-axial and bi-axial loading cases for square plates ($\frac{a}{b} = 1$) the optimum ply orientation was found for [0°/45°]s stacking sequence.
- For higher plate aspect ratios under uni-axial loading conditions, the optimum ply orientation was found for [0°/60°]s stacking sequence whereas for bi-axial loading the optimum ply orientation was found for cross-ply stacking sequence of [0°/90°]s.

Based on this study, it is paramount to state that pineapple leaf fibre-based composite materials exhibit better buckling characteristics than contemporary synthetic fibre composites such as E-glass composites. Thus, they have huge potential to be used in structural components under buckling conditions.

Nomenclature

E_{11}	Young's modulus in longitudinal direction (GPa)
E_{22}	Young's modulus in transverse direction (GPa)
ϑ_{12}	Major Poisson's ratio
ϑ_{21}	Minor Poisson's ratios
G_{12}	In-plane shear modulus
S_{ij}	Reduced compliance coefficients
Q_{ij}	Reduced stiffness coefficients
D_{ij}	Flexural stiffness
$[A]$	Extensional stiffness matrix
$[B]$	Coupling stiffness matrix
$[D]$	Bending stiffness matrix
σ	Stress (Pa or MPa)
τ	Shear stress (Pa or MPa)
ε	Strain
γ	Shear strain
W	Transverse displacement of a point on the plate
Λ	Natural frequency factor
ω	Natural frequency (Hz)
t	Time (s)
ρ	Density of the composite material (kg/m3)
f	Frequency (Hz)
N_o	Critical buckling load
$\overline{N}$	Non-dimensional buckling load
k	Plate buckling constant
ζ	Damping ratio
m	Half wavelengths in the x-direction
n	Half wavelengths in the y-direction
h	Total thickness of the laminate (mm)

N_{xy}	Stress resultants
a	Length of composite plate along x-axis (mm)
b	Breadth of composite plate along y-axis (mm)
U	Strain energy of plate
V	Potential energy in plate
Π	Total loss in potential energy of a deformed plate
δ	First variation according to Hamilton's principle

Acknowledgments

The authors want to thank the anonymous reviewers and all the persons concerned in helping with this paper.

Conflicts of Interest

The authors declare that there is no conflict of interest regarding the publication of this manuscript. In addition, the authors have entirely observed the ethical issues, including plagiarism, informed consent, misconduct, data fabrication and/or falsification, double publication and/or submission, and redundancy.

References

[1] Senthilkumar, K., Saba, N., Chandrasekar, M., Jawaid, M., Rajini, N., Alothman, O.Y. and Siengchin, S., 2019. Evaluation of mechanical and free vibration properties of the pineapple leaf fibre reinforced polyester composites. Construction and Building Materials, 195, pp.423-431.

[2] Saha, A., Kumar, S. and Kumar, A., 2021. Influence of pineapple leaf particulate on mechanical, thermal and biodegradation characteristics of pineapple leaf fiber reinforced polymer composite. Journal of Polymer Research, 28(2), pp.1-23.

[3] Peças, P., Carvalho, H., Salman, H. and Leite, M., 2018. Natural fibre composites and their applications: a review. Journal of composites science, 2(4), p.66.

[4] Mohammed, L., Ansari, M.N., Pua, G., Jawaid, M. and Islam, M.S., 2015. A review on natural fiber reinforced polymer composite and its applications. International journal of polymer science, 2015.

[5] Jawaid, M., Asim, M., Tahir, P.M. and Nasir, M., 2020. Pineapple Leaf Fibers.Springer Nature Singapore.

[6] Sema, A. and Maiti, C.S., 2010, July. Pineapple cultivation in north east India-a prospective venture. In VII International Pineapple Symposium 902 (pp. 69-78).

[7] Mishra, S., Misra, M., Tripathy, S.S., Nayak, S.K. and Mohanty, A.K., 2001. Potentiality of pineapple leaf fibre as reinforcement in PALF-polyester composite: Surface modification and mechanical performance. Journal of Reinforced Plastics and Composites, 20(4), pp.321-334.

[8] Borah, P.P., Kashyap, S., Kirtania, S. and Banerjee, S., 2022. Finite element and numerical analysis for structural responses of natural fibre-based epoxy composites. International Journal on Interactive Design and Manufacturing (IJIDeM), pp.1-13.

[9] Jalili, S., Khani, R. and Hosseinzadeh, Y., 2021, October. On the performance of flax fibres in multi-objective design of laminated composite plates for buckling and cost.In Structures (Vol. 33, pp. 3094-3106).Elsevier.

[10] Hosseinzadeh, Y., Jalili, S. and Khani, R., 2020. Investigating the effects of flax fibers application on multi-objective optimization of laminated composite plates for simultaneous cost minimization and frequency gap maximization. Journal of Building Engineering, 32, p.101477.

[11] Le, V.A., Zobeiry, N., Erkmen, E. and Malek, S., 2021. Buckling behaviour of laminated viscoelastic composites under axial loads. Mechanics of Materials, 159, p.103897.

[12] Le, V.A., Zobeiry, N., Erkmen, E. and Malek, S., 2019. Buckling analysis of multilayered beams with soft and rigid interfaces. In ICCM22 2019 (pp. 204-212). Melbourne, VIC: Engineers Australia.

[13] Chai, G.B. and Hoon, K.H., 1992. Buckling of generally laminated composite plates. Composites science and technology, 45(2), pp.125-133.

[14] Darvizeh, M., Darvizeh, A., Ansari, R. and Sharma, C.B., 2004. Buckling analysis of generally laminated composite plates (generalized differential quadrature rules versus Rayleigh–Ritz method). Composite Structures, 63(1), pp.69-74.

[15] Adali, S., 1995. Lay-up optimization of laminated plates under buckling loads. In Buckling and Postbuckling of Composite plates (pp. 329-365). Springer, Dordrecht.

[16] Bert, C.W. and Chen, T.L.C., 1976. Optimal design of composite material plates to resist buckling under biaxial compression. Transactions of the Japan Society for Composite Materials, 2, pp.7-10.

[17] Jones, R.M., 2014. Mechanics of composite materials. CRC press.

[18] Kazancı, Z. and Mecitoğlu, Z., 2008. Nonlinear dynamic behavior of simply

supported laminated composite plates subjected to blast load. Journal of Sound and Vibration, 317(3-5), pp.883-897.

[19] Reddy, J.N., 2003. Mechanics of laminated composite plates and shells: theory and analysis. CRC press.

[20] Komur, M.A., Sen, F., Ataş, A. and Arslan, N., 2010. Buckling analysis of laminated composite plates with an elliptical/circular cutout using FEM. Advances in Engineering Software, 41(2), pp.161-164.

[21] Kumar, K.V., Moshi, A.A.M. and Rajadurai, J.S., 2021. Mechanical property analysis on bamboo-glass fiber reinforced hybrid composite structures under different lamina orders. Materials Today: Proceedings, 45, pp.1620-1625.

[22] Faizan, M. and Gangwar, S., 2021. Tensile behaviour of carbon fiber reinforced polymer composite using ANSYS 21. Materials Today: Proceedings, 46, pp.6519-6526.

[23] Joshi, S.P. and Iyengar, N.G.R., 1985. Optimal design of laminated composite plates under axial compression. Transactions of the Canadian Society for Mechanical Engineering, 9(1), pp.45-50.